Rahaman and Raychowdhury *Geo-Engineering (2017)8:6*
DOI 10.1186/s40703-017-0040-4

International Journal of Geo-Engineering

RESEARCH Open Access

Seismic active earth pressure on bilinear retaining walls using a modified pseudo-dynamic method

Obaidur Rahaman[1,2] and Prishati Raychowdhury[2*]

*Correspondence:
prishati@iitk.ac.in
[2] Department of Civil Engineering, Indian Institute of Technology Kanpur, Kanpur, India
Full list of author information is available at the end of the article

Abstract

Background: Proper understanding of seismic behavior of retaining structures is crucial during a strong earthquake event. In particular, response of retaining walls with bilinear backface, where a sudden change in the inclination along its depth make the problem more complex. This study focuses on estimating the seismic earth pressure coefficients of a retaining wall with bilinear backface using a modified pseudo-dynamic method.

Methods: In this method, the backfill soil is modeled as a visco-elastic Kelvin–Voigt material. A frequency-dependant amplification function is derived for the waves traveling along the backfill using well-established one-dimensional ground response analysis theory. A rigorous parametric study has been carried out to understand the effect of various parameters such as amplitude of base acceleration, direction of vertical acceleration, soil shear resistance angle, soil-wall friction angle, wall inclination, frequency ratio, and damping ratio on the seismic active earth pressure.

Results: It has been observed that the damping ratio of the backfill soil plays an important role, particularly when the frequency of wave is close to the natural frequency of the backfill. Further, the seismic active thrust is found to increase in both upper and lower segments of the wall when the frequency of the primary wave is greater than that of the shear wave. Comparison of results with the previous studies indicates that the conventional pseudo-dynamic methods significantly underestimate the seismic coefficients and seismic pressures, particularly for the high-intensity motions.

Conclusions: The results of the study show that the natural frequency and damping of the backfill soil have significant effect on the seismic active earth pressure coefficients. Comparison with conventional pseudo-static and pseudo-dynamic methods indicates that the previous methods largely underestimate seismic coefficients and seismic pressures (as much as 48%). This under-estimation is more prominent for higher-intensity motions and less-damped soil, where the soil amplification effects pose most importance. This modified pseudo-dynamic approach can further be used for design of bilinear retaining structures.

Keywords: Pseudo-dynamic method, Bilinear retaining wall, Active earth pressure, Seismic behavior, Soil amplification

Background

In many practical situations, the backface of a retaining wall is made in such a way that it has an abrupt change in its inclination. For example, gabion type retaining walls (as shown in Fig. 1) are commonly used in the mountainous and remote areas where piecewise transportation of blocks is convenient [2]. However, during an earthquake, this sudden change in backface inclination may pose more complexity to the load carrying mechanism of the wall. Although a number of earlier studies had focused on static and dynamic analysis of vertical or non-vertical gravity or cantilever type retaining walls, consideration of bilinear backface is not common. Sokolovskii [12], in a pioneering work, carried out static analysis on retaining walls with bilinear backface. Later, Greco [5] developed an analytical solution to determine the static and pseudo-static active thrust on walls with bilinear backface. Sadrekarimi et al. [10] experimentally investigated the seismic lateral pressure behind a hunched-back gravity type quay wall. Kolathayar and Ghosh [7] focused on seismic active earth pressure behind a bilinear rigid cantilever retaining wall using pseudo-dynamic analysis. They had adopted the conventional pseudo-dynamic method originally proposed by Steedman and Zeng [13] and later updated by Choudhury and Nimbalkar [3]. However, this method has from some inherent limitations, such as, the seismic waves violate the zero stress boundary condition at the ground surface, the damping of the backfill is neglected, and arbitrary amplification factors are assumed. To overcome the above-mentioned deficiencies, the present study adopts a modified pseudo-dynamic method as suggested by Bellezza [1], where, the backfill soil is considered as a visco-elastic Kelvin–Voigt material and a frequency-dependant amplification of wave amplitudes along the height of the backfill has been accounted for.

Definition of the problem

Consider a rigid cantilever retaining wall with bilinear backface constructed on a rigid bedrock supporting a dry, horizontal and cohesionless backfill as shown in Fig. 2. The total height of the wall is H, and the upper part CD is of height H_1. The upper (CD) and

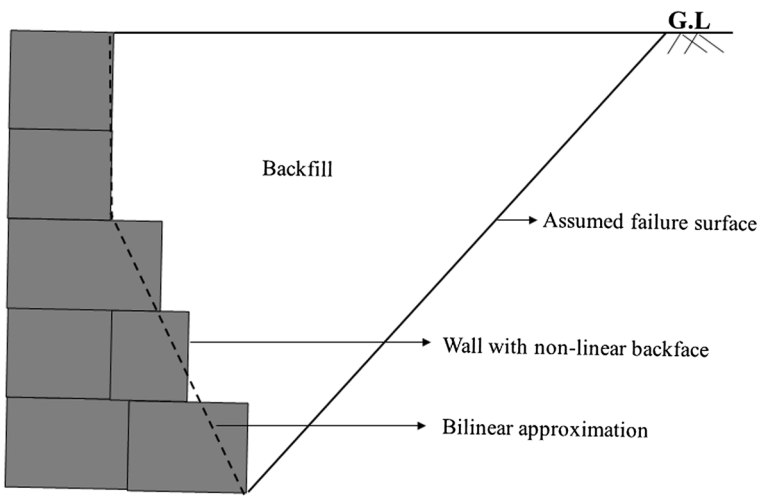

Fig. 1 Schematic of a retaining wall with non-linear backface

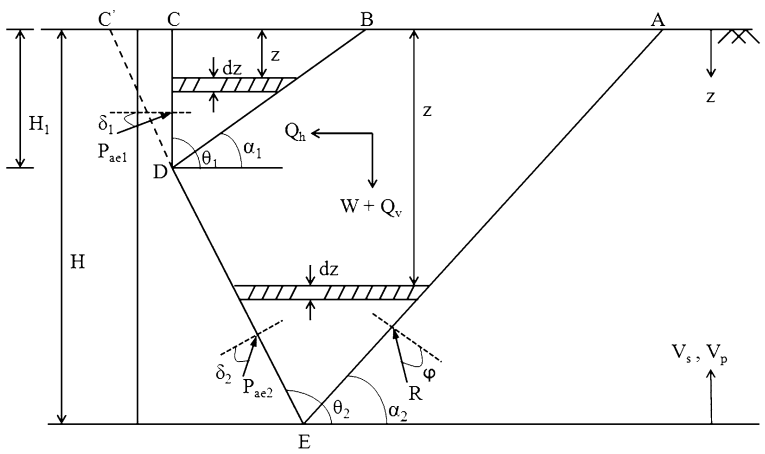

Fig. 2 Failure mechanism and forces acting on wall and backfill

lower (DE) segments are inclined at an angle θ_1 and θ_2, respectively, with the horizontal. The wall friction angles are δ_1 and δ_2, respectively, for the upper and lower portion of the wall. The base of the cantilever wall is subjected to a horizontal acceleration with magnitude a_{h0} and a vertical acceleration of magnitude a_{v0}. The backfill soil is considered as a visco-elastic Kelvin–Voigt material. The objective of this study is to determine the seismic active pressure coefficient for both upper and lower part of the wall and distribution of active pressure along the height of the wall.

Method of analysis

In this study, planar failure surfaces are assumed for both upper and lower segments of the wall, as suggested in Greco [5]. In the upper portion, the failure surface BD makes an angle α_1 with the horizontal, whereas, for the lower part, the failure surface AE makes an angle α_2 with the horizontal. The thrust wedge is subjected to its self-weight W. The active force P_{ae1} is inclined at an angle δ_1 with respect to the normal on CD, P_{ae2} is inclined at δ_2 with the normal on AE, and R is inclined at an angle φ with the normal to the failure surface AE.

Wave equation for a visco-elastic soil

The backfill soil is modeled as a visco-elastic Kelvin–Voigt material consisting of an elastic spring element and a viscous dashpot connected in parallel as shown in Fig. 3.

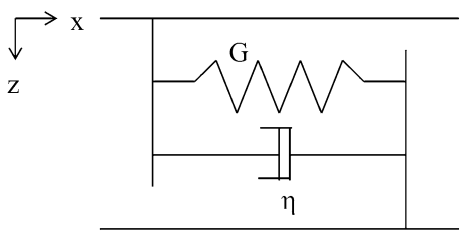

Fig. 3 Visco-elastic media of Kelvin–Voigt [8]

According to the definition of Kelvin–Voigt model, the constitutive equation of a visco-elastic medium is given by

$$\sigma_{xz} = 2G\varepsilon_{xz} + 2\eta\frac{\partial\varepsilon_{xz}}{\partial t} \tag{1}$$

where σ_{xz} is the shear stress, ε_{xz} is the shear strain, G is the shear modulus and η is the viscous damping coefficient. For a harmonic shaking, $\eta_s = 2GD/\omega$, where D is damping ratio and w is angular frequency. The motion equation of the Kelvin–Voigt visco-elastic medium (after [14]) is

$$\rho\frac{\partial^2 u}{\partial t^2} = \left\{(\lambda + G) + (\eta_1 + \eta_s)\frac{\partial}{\partial t}\right\}grad(\theta) + \left(G + \eta_s\frac{\partial}{\partial t}\right)\nabla^2 u \tag{2}$$

where ρ is the density of the media, λ and G are the Lame constant, η_1 and η_s are the viscosities, u is displacement vector with components along three different axis u_x, u_y and u_z, and $\theta = div(u)$. If the plane wave solution of wave propagating along the z-axis in the Kelvin–Voigt homogeneous visco-elastic medium is considered, then Eq. (2) can be simplified as the following two equations for horizontal and vertical displacement vectors:

$$\rho\frac{\partial^2 u_h}{\partial t^2} = G\frac{\partial^2 u_h}{\partial z^2} + \eta_s\frac{\partial^3 u_h}{\partial t\partial z^2} \tag{3}$$

and

$$\rho\frac{\partial^2 u_v}{\partial t^2} = (\lambda + 2G)\frac{\partial^2 u_v}{\partial z^2} + (\eta_1 + 2\eta_s)\frac{\partial^3 u_v}{\partial t\partial z^2} \tag{4}$$

The general solution of Eq. (3) for a harmonic wave is

$$u_h(z,t) = \exp(i\omega t)\left\{C_1\exp\left(-ik_s^* z\right) + C_2\exp\left(ik_s^* z\right)\right\} \tag{5}$$

where k_s^* is complex wave number defined as

$$k_s^* = \omega_s\sqrt{\rho/G^*} = k_{s1} + ik_{s2} \tag{6}$$

where G^* is complex shear modulus and given by

$$G^* = G + i\omega\eta_s = G(1 + 2D_s i) \tag{7}$$

By applying the boundary conditions that is shear stress at the free surface ($z = 0$) is zero and at $z = H$ the displacement will be equal to the rigid base ($u_{bh} = u_{h0}\exp(i\omega t)$), the horizontal displacement is expressed as

$$u_h(z,t) = u_{h0}\exp(i\omega t)\frac{\cos\left(k_s^* z\right)}{\cos\left(k_s^* H\right)} \tag{8}$$

Taking only the real part, Eq. (8) can be expressed as

$$u_h(z,t) = \frac{u_{h0}}{C_s^2 + S_s^2}\left[(C_s C_{sz} + S_s S_{sz})\cos(w_s t) + (S_s C_{sz} - C_s S_{sz})\sin(w_s t)\right] \tag{9}$$

The horizontal acceleration can be obtained

$$a_h(z,t) = \frac{a_{h0}}{C_s^2 + S_s^2}[(C_s C_{sz} + S_s S_{sz})\cos(w_s t) + (S_s C_{sz} - C_s S_{sz})\sin(w_s t)] \quad (10)$$

Similarly, the vertical acceleration is obtained as

$$a_v(z,t) = \frac{a_{v0}}{C_p^2 + S_p^2}\left[\left(C_p C_{pz} + S_p S_{pz}\right)\cos\left(w_p t\right) + \left(S_p C_{pz} + C_p S_{pz}\right)\sin\left(w_p t\right)\right] \quad (11)$$

where

$$C_{sz} = \cos\left(y_{s1} z/H\right)\cosh\left(y_{s2} z/H\right)$$

$$C_{pz} = \cos\left(y_{p1} z/H\right)\cosh\left(y_{p2} z/H\right)$$

$$S_{sz} = -\sin\left(y_{s1} z/H\right)\sinh\left(y_{s2} z/H\right)$$

$$S_{pz} = -\sin\left(y_{p1} z/H\right)\sinh\left(y_{p2} z/H\right)$$

$$C_s = \cos\left(y_{s1}\right)\cosh\left(y_{s2}\right)$$

$$C_p = \cos\left(y_{p1}\right)\cosh\left(y_{p2}\right)$$

$$S_s = -\sin\left(y_{s1}\right)\sinh\left(y_{s2}\right)$$

$$S_p = -\sin\left(y_{p1}\right)\sinh\left(y_{p2}\right)$$

$$y_{s1} = k_{s1}H = \frac{w_s H}{V_s}\sqrt{\frac{\sqrt{1+4D_s^2}+1}{2\left(1+4D_s^2\right)}}$$

$$y_{p1} = k_{p1}H = \frac{w_p H}{V_p}\sqrt{\frac{\sqrt{1+4D_p^2}+1}{2\left(1+4D_p^2\right)}}$$

$$y_{s2} = k_{s2}H = -\frac{w_s H}{V_s}\sqrt{\frac{\sqrt{1+4D_s^2}-1}{2\left(1+4D_s^2\right)}}$$

$$y_{p2} = k_{p2}H = -\frac{w_p H}{V_p}\sqrt{\frac{\sqrt{1+4D_p^2}-1}{2\left(1+4D_p^2\right)}}$$

where k_{s1} and k_{s2} are the real and imaginary parts of complex wave number k_s^*, k_{p1} and k_{p2} real and imaginary parts of k_p^*, is the first Lame's constant, D_s and D_p are damping ratios and ω_p and ω_s are angular frequencies for shear and primary wave, respectively.

Estimation of active thrust for the upper segment (CD)

To estimate the active earth pressure on the upper segment, the equilibrium of the soil wedge BCD has been considered. The mass of the thin element of thickness dz at depth z in wedge BCD is given by

$$m_1(z) = \frac{\gamma}{g}(H_1 - z)(\cot\alpha_1 - \cot\theta_1)dz \tag{12}$$

where γ is unit weight of the backfill soil and g is acceleration due to gravity. The total weight of wedge BCD is computed by integrating Eq. (12) as

$$W_1 = \int_0^{H_1} m_1(z)dz = \frac{\gamma H_1^2}{2}(\cot\alpha_1 - \cot\theta_1) \tag{13}$$

The total horizontal inertial force (Q_{h1}) and vertical inertial force (Q_{v1}) on the wedge BCD are given by

$$Q_{h1}(t,\alpha_1) = \int_{z=0}^{z=H_1} a_h(z,t)m(z) = \int_{z=0}^{z=H_1} a_h(z,t)\frac{\gamma}{g}(H_1 - z)(\cot\alpha_1 - \cot\theta_1)dz \tag{14}$$

$$Q_{v1}(t,\alpha_1) = \int_{z=0}^{z=H_1} \alpha_v(z,t)m(z) = \int_{z=0}^{z=H_1} \alpha_v(z,t)\frac{\gamma}{g}(H_1 - z)(\cot\alpha_1 - \cot\theta_1)dz \tag{15}$$

The total horizontal inertial force (Q_{h1}) and vertical inertial force (Q_{v1}) can be expressed as

$$Q_{h1}(t,\alpha_1) = \frac{a_{h0}}{g}\gamma H_1^2(\cot\alpha_1 - \cot\theta_1)[A_{hu}\cos(w_s t) + B_{hu}\sin(w_s t)] \tag{16}$$

$$Q_{v1}(t,\alpha_1) = \frac{a_{v0}}{g}\gamma H_1^2(\cot\alpha_1 - \cot\theta_1)\left[A_{vu}\cos\left(w_p t\right) + B_{vu}\sin\left(w_p t\right)\right] \tag{17}$$

where the dimensionless coefficients A_{hu}, B_{hu}, A_{vu} and B_{vu} are given by

$$A_{hu} = \frac{2y_{s1u}y_{s2u}\sin\left(y_{s1u}\right)\sinh\left(y_{s2u}\right) + \left(y_{s1u}^2 - y_{s2u}^2\right)\left\{\cos\left(y_{s1u}\right)\cosh\left(y_{s2u}\right) - \cos^2\left(y_{s1u}\right) - \sinh^2\left(y_{s2u}\right)\right\}}{\left\{\cos^2\left(y_{s1u}\right) + \sinh^2\left(y_{s2u}\right)\right\}\left(y_{s1u}^2 + y_{s2u}^2\right)^2}$$

$$B_{hu} = \frac{2y_{s1u}y_{s2u}\left\{\cos\left(y_{s1u}\right)\cosh\left(y_{s2u}\right) - \cos^2\left(y_{s1u}\right) - \sinh^2\left(y_{s2u}\right)\right\} - \left(y_{s1u}^2 - y_{s2u}^2\right)\sin\left(y_{s1u}\right)\sinh\left(y_{s2u}\right)}{\left\{\cos^2\left(y_{s1u}\right) + \sinh^2\left(y_{s2u}\right)\right\}\left(y_{s1u}^2 + y_{s2u}^2\right)^2}$$

$$A_{vu} = \frac{2y_{p1u}y_{p2u}\sin\left(y_{p1u}\right)\sinh\left(y_{p2u}\right) + \left(y_{p1u}^2 - y_{p2u}^2\right)\left\{\cos\left(y_{p1u}\right)\cosh\left(y_{p2u}\right) - \cos^2\left(y_{p1u}\right) - \sinh^2\left(y_{p2u}\right)\right\}}{\left\{\cos^2\left(y_{p1u}\right) + \sinh^2\left(y_{p2u}\right)\right\}\left(y_{p1u}^2 + y_{p2u}^2\right)^2}$$

$$B_{vu} = \frac{2y_{p1u}y_{p2u}\left\{\cos\left(y_{p1u}\right)\cosh\left(y_{p2u}\right) - \cos^2\left(y_{p1u}\right) - \sinh^2\left(y_{p2u}\right)\right\} - \left(y_{p1u}^2 - y_{p2u}^2\right)\sin\left(y_{p1u}\right)\sinh\left(y_{p2u}\right)}{\left\{\cos^2\left(y_{p1u}\right) + \sinh^2\left(y_{p2u}\right)\right\}\left(y_{p1u}^2 + y_{p2u}^2\right)^2}$$

also $y_{s1u} = k_{s1}H_1$, $y_{s2u} = k_{s2}H_1$, $y_{p1u} = k_{p1}H_1$ and $y_{p2u} = k_{p2}H_1$.

Assuming the wedge BCD is in limit equilibrium condition and considering the vertical and horizontal equilibrium of the wedge, the total active thrust on the upper portion of the wall is obtained using the following equation

$$P_{ae1}(\alpha_1, t) = \frac{W_1\sin\left(\alpha_1 - \varphi\right)}{\sin\left(\delta_1 + \theta_1 + \varphi - \alpha_1\right)} + \frac{Q_{h1}\cos\left(\alpha_1 - \varphi\right) + Q_{v1}\sin\left(\alpha_1 - \varphi\right)}{\sin\left(\delta_1 + \theta_1 + \varphi - \alpha_1\right)} \tag{18}$$

The maximum value of Eq. (18) with respect to α_1 and t can be considered as the estimated seismic active pressure on the wall. Substituting Eqs. (13), (16) and (17) in Eq. (18)

$$P_{ae1,\max} = \max\left\{\begin{array}{l} \frac{\gamma H_1^2}{2}\frac{\sin(\alpha_1-\varphi)(\cot\alpha_1-\cot\theta_1)}{\sin(\delta_1+\theta_1+\varphi-\alpha_1)} \\ +\frac{a_{h0}}{g}\gamma H_1^2\frac{\cos(\alpha_1-\varphi)(\cot\alpha_1-\cot\theta_1)}{\sin(\delta_1+\theta_1+\varphi-\alpha_1)}\left[A_{hu}\cos\left(w_s t\right) + B_{hu}\sin\left(w_s t\right)\right] \\ +\frac{a_{v0}}{g}\gamma H_1^2\frac{\sin(\alpha_1-\varphi)(\cot\alpha_1-\cot\theta_1)}{\sin(\delta_1+\theta_1+\varphi-\alpha_1)}\left[A_{vu}\cos\left(w_p t\right) + B_{vu}\sin\left(w_p t\right)\right] \end{array}\right\} \tag{19}$$

The seismic active earth pressure coefficient can be obtained by the following equation

$$K_{ae1} = \frac{2P_{ae1,\max}}{\gamma H_1^2} = \left\{\begin{array}{l} \frac{\sin(\alpha_{1m}-\varphi)(\cot\alpha_{1m}-\cot\theta_1)}{\sin(\delta_1+\theta_1+\varphi-\alpha_{1m})} \\ +\frac{2a_{h0}}{g}\frac{\cos(\alpha_{1m}-\varphi)(\cot\alpha_{1m}-\cot\theta_1)}{\sin(\delta_1+\theta_1+\varphi-\alpha_{1m})}\left[A_{hu}\cos\left(w_s t_m\right) + B_{hu}\sin\left(w_s t_m\right)\right] \\ +\frac{2a_{v0}}{g}\frac{\sin(\alpha_{1m}-\varphi)(\cot\alpha_{1m}-\cot\theta_1)}{\sin(\delta_1+\theta_1+\varphi-\alpha_{1m})}\left[A_{vu}\cos\left(w_p t_m\right) + B_{vu}\sin\left(w_p t_m\right)\right] \end{array}\right\} \tag{20}$$

where α_{1m} and t_m are the values of α_1 and t that maximizes K_{ae1}.

Estimation of active thrust for the lower segment (DE)

For determination of active pressure on the lower part,the contribution of the entire wedge ABCDE has to be considered. The mass of the thin element of thickness dz at depth z in wedge ABCDE as shown in Fig. 2 is given by

$$m_2(z) = m_{21}(z) - m_{22}(z) \tag{21}$$

where $m_{21}(z)$ is the mass of wedge ABC′DE, expressed as

$$m_{21}(z) = \frac{\gamma}{g}(H - z)(\cot\alpha_2 - \cot\theta_2)dz \quad 0 \le z \le H \tag{22}$$

and $m_{22}(z)$ which is the mass of wedge CC′D, is given by

$$m_{22}(z) = \frac{\gamma}{g}(H_1 - z)(\cot\theta_1 - \cot\theta_2)dz \quad 0 \le z \le H_1 \tag{23}$$

The total weight of wedge ABCDE can be derived as

$$W_2 = \int_{z=0}^{z=H} m_{21}(z) - \int_{z=0}^{z=H_1} m_{22}(z) = \frac{\gamma}{2}\left[H^2(\cot\alpha_2 - \cot\theta_2) - H_1^2(\cot\theta_1 - \cot\theta_2)\right] \quad (24)$$

The total horizontal inertial force (Q_{h2}) and vertical inertial force (Q_{v2}) on the wedge ABCDE are given by

$$Q_{h2}(t,\alpha_2) = \int_{z=0}^{z=H} a_h(z,t)m_{21}(z) - \int_{z=0}^{z=H_1} a_h(z,t)m_{22}(z) \quad (25)$$

$$Q_{v2}(t,\alpha_2) = \int_{z=0}^{z=H} \alpha_v(z,t)m_{21}(z) - \int_{z=0}^{z=H_1} \alpha_v(z,t)m_{22}(z) \quad (26)$$

The total active thrust on the lower portion of the wall is obtained by imposing the vertical and horizontal equilibrium of the wedge ABCDE, assuming the wedge is in limit equilibrium condition and it is expressed as

$$P_{ae2}(\alpha_2,t) = \left\{ \begin{array}{l} \frac{W_2\sin(\alpha_2-\varphi)}{\sin(\delta_2+\theta_2+\varphi-\alpha_2)} + \frac{Q_{h2}\cos(\alpha_2-\varphi)+Q_{v2}\sin(\alpha_2-\varphi)}{\sin(\delta_2+\theta_2+\varphi-\alpha_2)} \\ -\frac{P_{ae1}(\alpha_1,t)\sin(\delta_1+\theta_1+\varphi-\alpha_2)}{\sin(\delta_2+\theta_2+\varphi-\alpha_2)} \end{array} \right\} \quad (27)$$

Also, the seismic active earth pressure coefficient for the lower portion can be obtained by the following equation

$$K_{ae2} = \frac{2P_{ae2,\max}}{\gamma H^2} \quad (28)$$

Estimation of active earth pressure distribution

The seismic active earth pressure distribution can be obtained by writing P_{ae1} and P_{ae2} as functions of z instead of H, and then partially differentiating them with respect to z [13]. By normalizing active pressure distribution (p_{ae1}) along the upper segment with respect to γH, $\frac{p_{ae1}}{\gamma H}$ is expressed as

$$\frac{p_{ae1}}{\gamma H} = \left\{ \begin{array}{l} \frac{z}{H}(\cot\alpha_1 - \cot\theta_1)\frac{\sin(\alpha_1-\varphi)}{\sin(\delta_1+\theta_1+\varphi-\alpha_1)} \\ +\frac{a_{h0}}{g}(\cot\alpha_1 - \cot\theta_1)\left[A_{ph}\cos(\omega_s t) + B_{ph}\sin(\omega_s t)\right]\frac{\cos(\alpha_1-\varphi)}{\sin(\delta_1+\theta_1+\varphi-\alpha_1)} \\ +\frac{a_{v0}}{g}(\cot\alpha_1 - \cot\theta_1)\left[A_{pv}\cos(\omega_p t) + B_{pv}\sin(\omega_p t)\right]\frac{\sin(\alpha_1-\varphi)}{\sin(\delta_1+\theta_1+\varphi-\alpha_1)} \end{array} \right\} \quad (29)$$

where,

$$A_{ph} = \frac{\left(C_s y_{s2} + S_s y_{s1}\right)\cos\left(y_{s1}\frac{z}{H}\right)\sinh\left(y_{s2}\frac{z}{H}\right) + \left(C_s y_{s1} - S_s y_{s2}\right)\sin\left(y_{s1}\frac{z}{H}\right)\cosh\left(y_{s2}\frac{z}{H}\right)}{\left(C_s^2 + S_s^2\right)\left(y_{s1}^2 + y_{s2}^2\right)}$$

$$B_{ph} = \frac{\left(S_s y_{s2} - C_s y_{s1}\right)\cos\left(y_{s1}\frac{z}{H}\right)\sinh\left(y_{s2}\frac{z}{H}\right) + \left(S_s y_{s1} + C_s y_{s2}\right)\sin\left(y_{s1}\frac{z}{H}\right)\cosh\left(y_{s2}\frac{z}{H}\right)}{\left(C_s^2 + S_s^2\right)\left(y_{s1}^2 + y_{s2}^2\right)}$$

$$A_{pv} = \frac{\left(C_p y_{p2} + S_p y_{p1}\right) \cos\left(y_{p1}\frac{z}{H}\right) \sinh\left(y_{p2}\frac{z}{H}\right) + \left(C_p y_{p1} - S_p y_{p2}\right) \sin\left(y_{p1}\frac{z}{H}\right) \cosh\left(y_{p2}\frac{z}{H}\right)}{\left(C_p^2 + S_p^2\right)\left(y_{p1}^2 + y_{p2}^2\right)}$$

$$B_{pv} = \frac{\left(S_p y_{p2} - C_p y_{p1}\right) \cos\left(y_{p1}\frac{z}{H}\right) \sinh\left(y_{p2}\frac{z}{H}\right) + \left(S_p y_{p1} + C_p y_{p2}\right) \sin\left(y_{p1}\frac{z}{H}\right) \cosh\left(y_{p2}\frac{z}{H}\right)}{\left(C_p^2 + S_p^2\right)\left(y_{p1}^2 + y_{p2}^2\right)}$$

Similarly, for the lower segment, the normalized active earth pressure distribution is expressed as

$$\frac{p_{ae2}}{\gamma H} = \left\{ \begin{array}{l} \left[\frac{z}{H}(\cot\alpha_2 - \cot\theta_2) - \frac{H_1}{H}(\cot\theta_1 - \cot\theta_2)\right] \frac{\sin(\alpha_2 - \varphi)}{\sin(\delta_2 + \theta_2 + \varphi - \alpha_2)} \\ + \frac{\alpha_{h0}}{g}\left[\begin{array}{l}(\cot\alpha_2 - \cot\theta_2)\{A_{ph}\cos(\omega_s t) + B_{ph}\sin(\omega_s t)\} \\ (\cot\theta_1 - \cot\theta_2)\{C_{ph}\cos(\omega_s t) + D_{ph}\sin(\omega_s t)\}\end{array}\right] \frac{\cos(\alpha_2 - \varphi)}{\sin(\delta_2 + \theta_2 + \varphi - \alpha_2)} \\ + \frac{\alpha_{v0}}{g}\left[\begin{array}{l}(\cot\alpha_2 - \cot\theta_2)\{A_{pv}\cos(\omega_p t) + B_{pv}\sin(\omega_p t)\} \\ (\cot\theta_1 - \cot\theta_2)\{C_{pv}\cos(\omega_p t) + D_{pv}\sin(\omega_p t)\}\end{array}\right] \frac{\sin(\alpha_2 - \varphi)}{\sin(\delta_2 + \theta_2 + \varphi - \alpha_2)} \end{array} \right\} \quad (30)$$

where,

$$C_{ph} = \frac{\left(C_s y_{s2} + S_s y_{s1}\right) \cos\left(y_{s1}\frac{H_1}{H}\right) \sinh\left(y_{s2}\frac{H_1}{H}\right) + \left(C_s y_{s1} - S_s y_{s2}\right) \sin\left(y_{s1}\frac{H_1}{H}\right) \cosh\left(y_{s2}\frac{H_1}{H}\right)}{\left(C_s^2 + S_s^2\right)\left(y_{s1}^2 + y_{s2}^2\right)}$$

$$D_{ph} = \frac{\left(S_s y_{s2} - C_s y_{s1}\right) \cos\left(y_{s1}\frac{H_1}{H}\right) \sinh\left(y_{s2}\frac{H_1}{H}\right) + \left(S_s y_{s1} + C_s y_{s2}\right) \sin\left(y_{s1}\frac{H_1}{H}\right) \cosh\left(y_{s2}\frac{H_1}{H}\right)}{\left(C_s^2 + S_s^2\right)\left(y_{s1}^2 + y_{s2}^2\right)}$$

$$C_{pv} = \frac{\left(C_p y_{p2} + S_p y_{p1}\right) \cos\left(y_{p1}\frac{H_1}{H}\right) \sinh\left(y_{p2}\frac{H_1}{H}\right) + \left(C_p y_{p1} - S_p y_{p2}\right) \sin\left(y_{p1}\frac{H_1}{H}\right) \cosh\left(y_{p2}\frac{H_1}{H}\right)}{\left(C_p^2 + S_p^2\right)\left(y_{p1}^2 + y_{p2}^2\right)}$$

$$D_{pv} = \frac{\left(S_p y_{p2} - C_p y_{p1}\right) \cos\left(y_{p1}\frac{H_1}{H}\right) \sinh\left(y_{p2}\frac{H_1}{H}\right) + \left(S_p y_{p1} + C_p y_{p2}\right) \sin\left(y_{p1}\frac{H_1}{H}\right) \cosh\left(y_{p2}\frac{H_1}{H}\right)}{\left(C_p^2 + S_p^2\right)\left(y_{p1}^2 + y_{p2}^2\right)}$$

Results and discussion

The maximum seismic active earth pressure coefficients for both upper and lower segments have been determined by optimizing Eq. (20) and (28) with respect to α_1, α_2 and t/T. In this analysis, the damping ratio of soil during propagation of shear wave and primary wave are assumed to be same, i.e., $D_s = D_p = D$. Further, the soil-wall friction angle for both upper and lower segments are assumed to be equal, i.e. $\delta_1 = \delta_2 = \delta$. Poisson's ratio of the backfill soil is assumed as 0.3, which gives the ratio of P-wave and S-wave velocity (V_p/V_s) approximately 1.87 [4, 8]. The effect of various parameters are investigated on three response parameters, namely, seismic active earth pressure coefficients, seismic earth pressure distribution over the height of the wall, and failure angle. Note that the damping ratio of 10% is assumed in the present analysis. Further, to understand the effect of damping on the earth pressure, additional analyses with 10, 20 and

30% damping values are conducted. For a dense sand and a medium-level excitation (this study considers a 0.2 g acceleration intensity), this damping range is a reasonable assumption as per the existing literature (for example, [6, 11]).

The following subsections discuss this parametric study on the above-mentioned response parameters. A more detailed description is available in the master's thesis of the first author, Rahaman [9].

Seismic active earth pressure coefficients

Effect of input frequency and damping ratio

Figure 4 shows the variation of K_{ae1} and K_{ae2} with normalized angular frequency for different damping ratios assuming $H_1/H = 1/3$, $\varphi = 40°$, $\delta = 0.5\ \varphi$ $\theta_1 = 75°$, $\theta_2 = 100°$, $a_{h0}/g = 0.2$ $a_{v0} = 0$ and $\omega_p/\omega_s = 1$. It can be observed that the trend of the curve is not monotonic and there is a distinct increase for $\omega_s H/V_s = 1.57$. After a sharp increase, the curve decreases monotonically. These peaks correspond to the resonance, i.e., the frequency of the incident wave is close to the natural frequency of the backfill. It is also observed that the damping ratio has significant effect on the seismic active earth pressure coefficient near these amplification zones. The peak value of K_{ae1} and K_{ae2} decrease about 30 and 35%, respectively, for increase in damping ratio from 20 to 30%. Note that the effect of backfill damping is not significant beyond $\omega_s H/V_s \geq 2$ and $\omega_s H/V_s \leq 0.5$.

Effect of horizontal and vertical acceleration

Figure 5 shows the variations of K_{ae1} and K_{ae2} with horizontal acceleration, a_{h0}/g for two conditions: (1) Q_v acting downward and (2) Q_v acting upward. It is observed that the horizontal seismic acceleration coefficients for both the segments increase monotonically as the horizontal inertia force on the backfill increases with increasing horizontal acceleration. It is obvious that the direction of acceleration during earthquake is not fixed; rather it changes its direction from cycle to cycle. This may subsequently cause a change in the direction of the seismic body forces with time. For evaluation of active earth pressure, the horizontal force must have to act towards the direction of wall face but the vertical force may act in upward or downward direction. Hence, there is always a phase difference between the horizontal seismic force and the vertical seismic force. The different directions of Q_v imply that when the active thrust reaches its maximum for Q_h, the Q_v may either have a positive or a negative value. Hence, K_{ae1} and K_{ae2} may have different values for the same magnitude of Q_v. The critical direction of the vertical force depends on many parameters, such as, soil friction angle, horizontal acceleration, non-dimensional frequency ratio and damping ratio of soil. It can be seen from Fig. 5 that for $\omega_s H/V_s = 0.5$, the critical condition for active thrust occurs when Q_v acts downward for low intensity motions (low range of a_{h0}/g). However, for high intensity motions, upward is more critical. This change in scenario happens at $a_{h0}/g = 0.3$ for K_{ae1}, and at $a_{h0}/g = 0.37$ for K_{ae2}. When plotted with normalized frequency ratio (Fig. 6), it is noted that the critical direction of vertical acceleration changes when the normalized frequency of the shear wave approaches the natural frequency of the backfill. Hence, it can be concluded from the above observations that the direction of vertical seismic force has significant effect on critical values of K_{ae1} and K_{ae2}, and should be given required importance while estimating the seismic earth pressures.

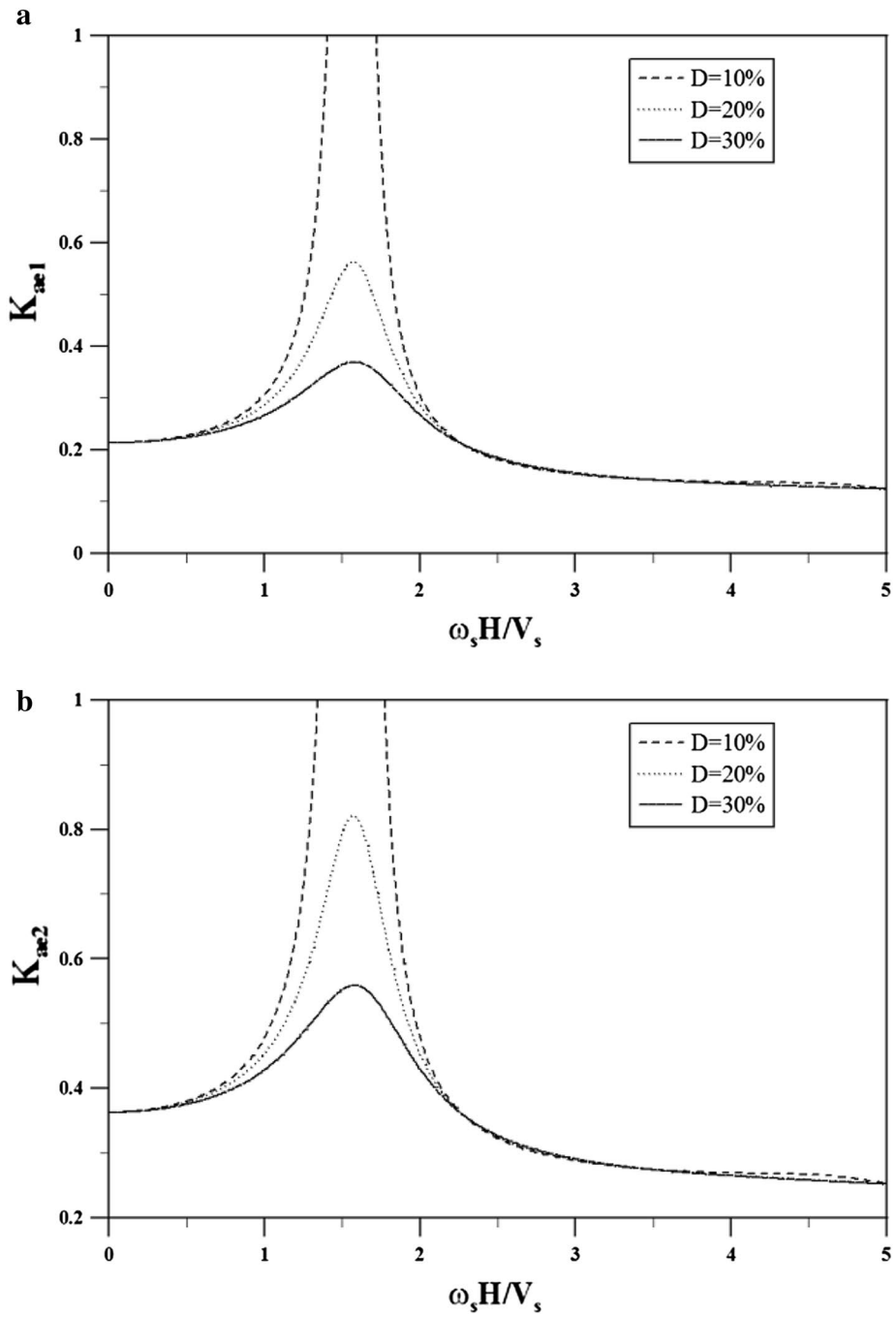

Fig. 4 Variation of active earth pressure coefficients with normalized angular frequency [for $H_1/H = 1/3$, $\varphi = 40°$, $\delta = 0.5\,\varphi$, $\theta_1 = 75°$, $\theta_2 = 100°$, $a_{h0}/g = 0.2$, $a_{v0} = 0$ and $\omega_p/\omega_s = 1$]. **a** K_{ae1}, **b** K_{ae2}

Effect of soil friction angle

Figure 7 demonstrates that the magnitude of K_{ae1} and K_{ae2} are significantly affected by the internal friction angle of the backfill soil. As expected, with increase in friction angle, soil gets denser and stiffer and thus reduce the active earth pressure coefficients. For

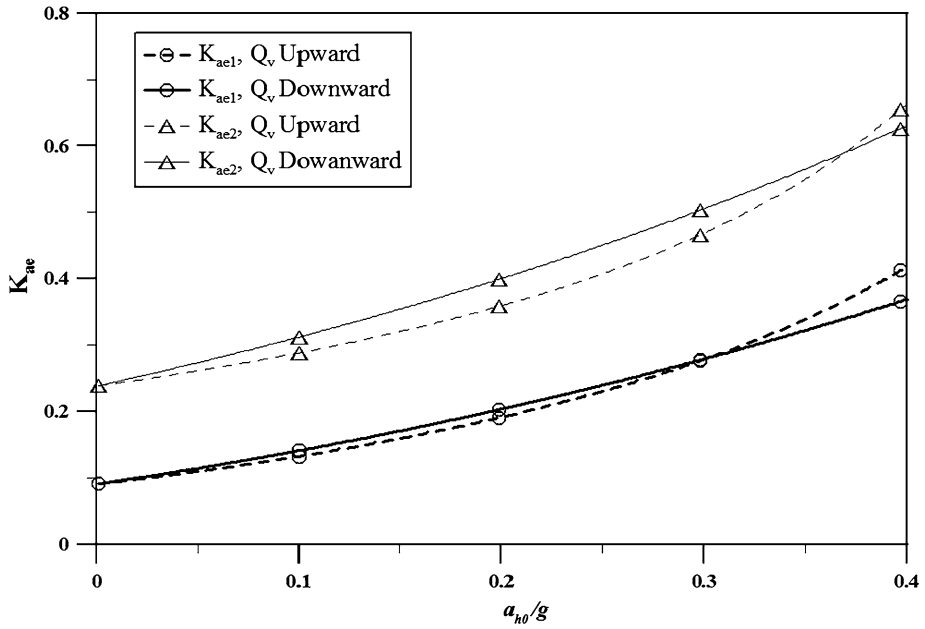

Fig. 5 Variation of active earth pressure coefficients with horizontal seismic acceleration coefficient [for $H_1/H = 1/3\ \varphi, = 40°, \delta = 0.5\ \varphi, \theta_1 = 75°, \theta_2 = 100°, a_{v0} = 0.5a_{h0}, \omega_s H/V_s = 0.5, D = 10\%$ and $\omega_p/\omega_s = 1$]

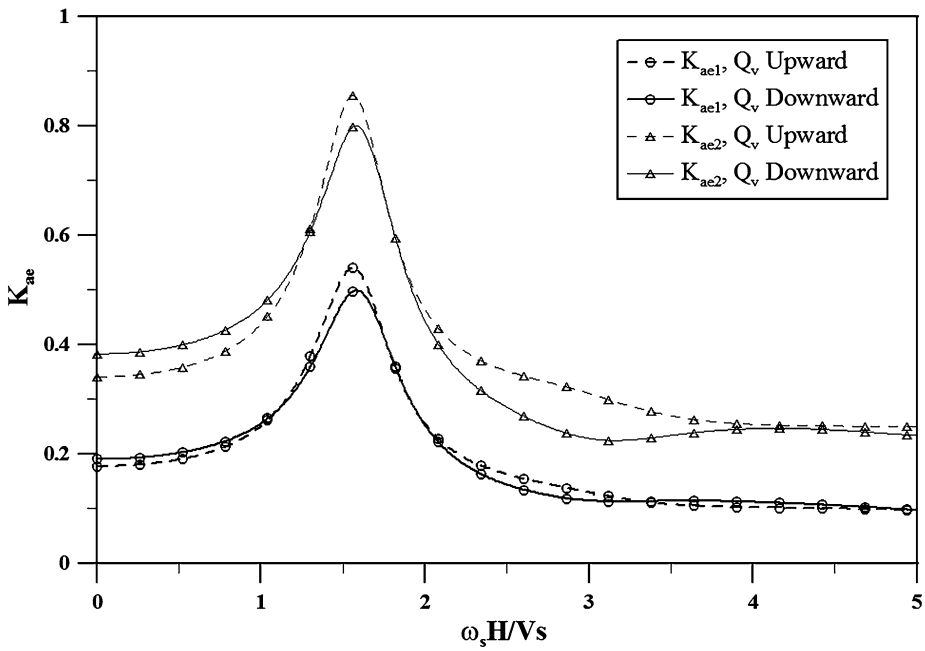

Fig. 6 Variation of active earth pressure coefficients with normalized frequency ratio [for $H_1/H = 1/3, \varphi = 40°, \delta = 0.5\ \varphi, \theta_1 = 75°, \theta_2 = 100°, a_{h0}/g = 0.2, a_{v0} = 0.5a_{h0}, D = 20\%$ and $\omega_p/\omega_s = 1$]

example, at $a_{h0}/g = 0.2$, with an increase in φ from 40° to 50°, K_{ae1} and K_{ae2} decrease by about 38 and 22%, respectively. The rate of effect of φ is more prominent for higher intensity motions, i.e., for greater values of a_{h0}/g.

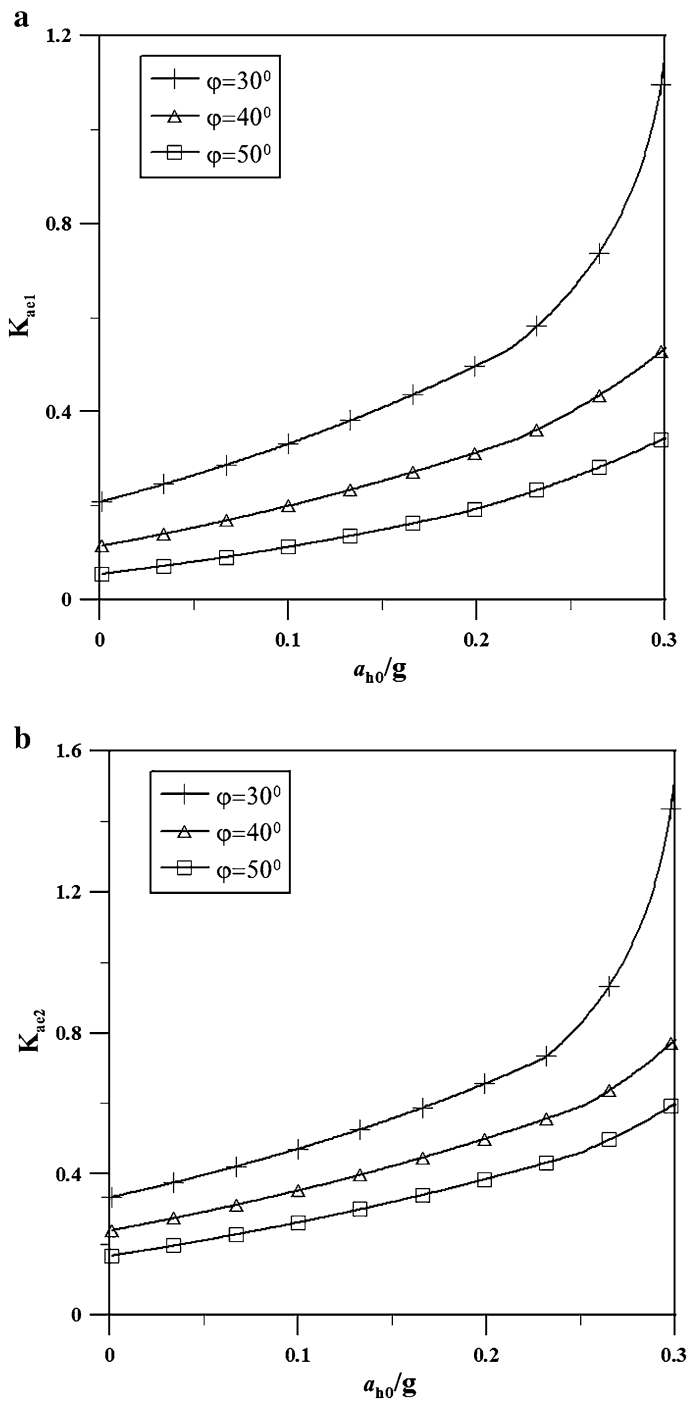

Fig. 7 Effect of friction angle on active earth pressure coefficients [for $H_1/H = 1/3$, $\delta = 0.5\,\varphi$, $\theta_1 = 75°$, $\theta_2 = 100°$, $|a_{v0}| = 0.5a_{h0}$, $\omega_s H/V_s = 2$, $D = 10\%$ and $\omega_p/\omega_s = 1$]. **a** K_{ae1}, **b** K_{ae2}

Effect of inclination angle

The influence of inclination angle of upper part of the bilinear wall (θ_1), on active earth pressure coefficients has been shown in Fig. 8. It can be noticed that K_{ae1} increases significantly with increasing θ_1, while K_{ae2} varies only marginally. For example, at $a_{h0}/g = 0.2$,

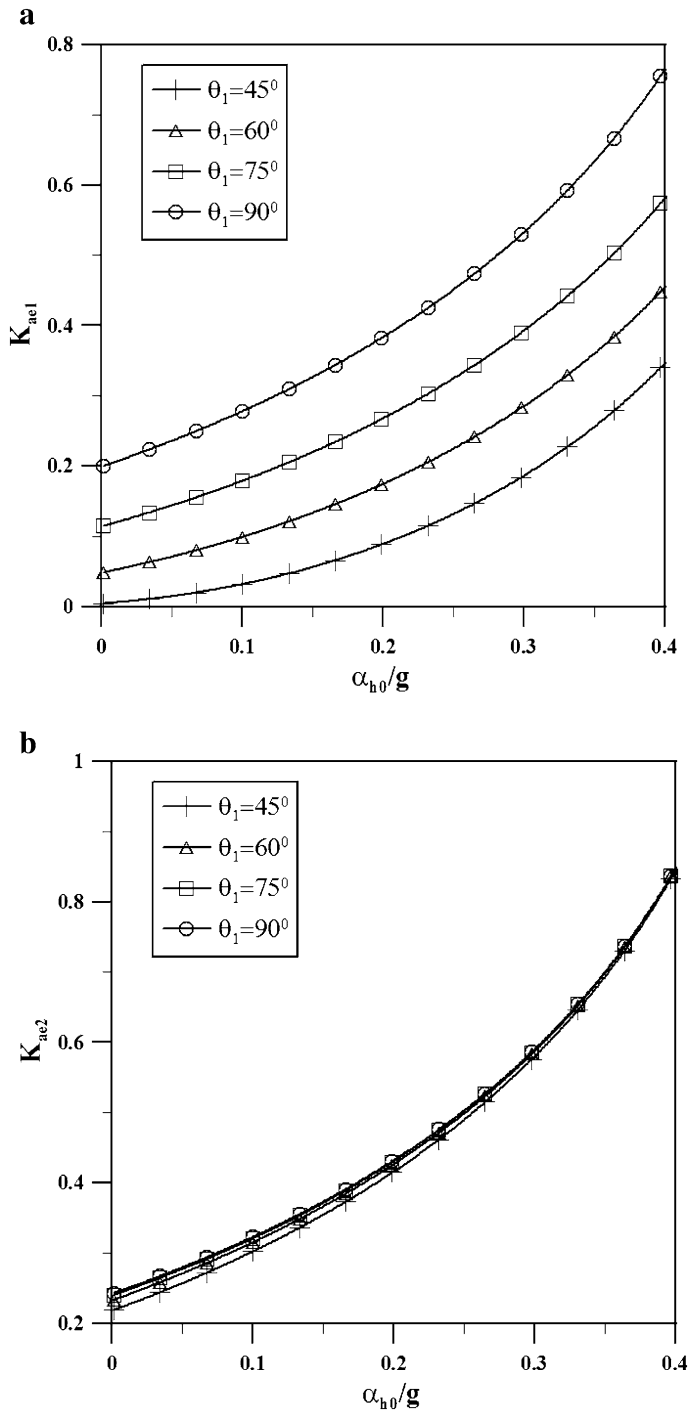

Fig. 8 Effect of inclination of top segment on active earth pressure coefficients [for $H_1/H = 1/3$, $\varphi = 40°$, $\delta = 0.5\,\varphi$, $\theta_2 = 100°$, $|a_{v0}| = 0.5a_{h0}$, $\omega_s H/V_s = 2$, $D = 30\%$ and $\omega_p/\omega_s = 1$]. **a** K_{ae1}, **b** K_{ae2}

with an increase of θ_1 from 60° to 75°, K_{ae1} increases from 0.175 to 0.268 (53% increase), whereas K_{ae2} increases from 0.427 to 0.431 (only 1%). It is expected that the inclination of upper part would influence the coefficient corresponding to the upper part and vice

versa. When the inclination angle of the lower segment of the wall (θ_2) is considered, just an opposite trend is observed, i.e., sensitivity of K_{ae2} over K_{ae1} in this case, as also expected (Fig. 9).

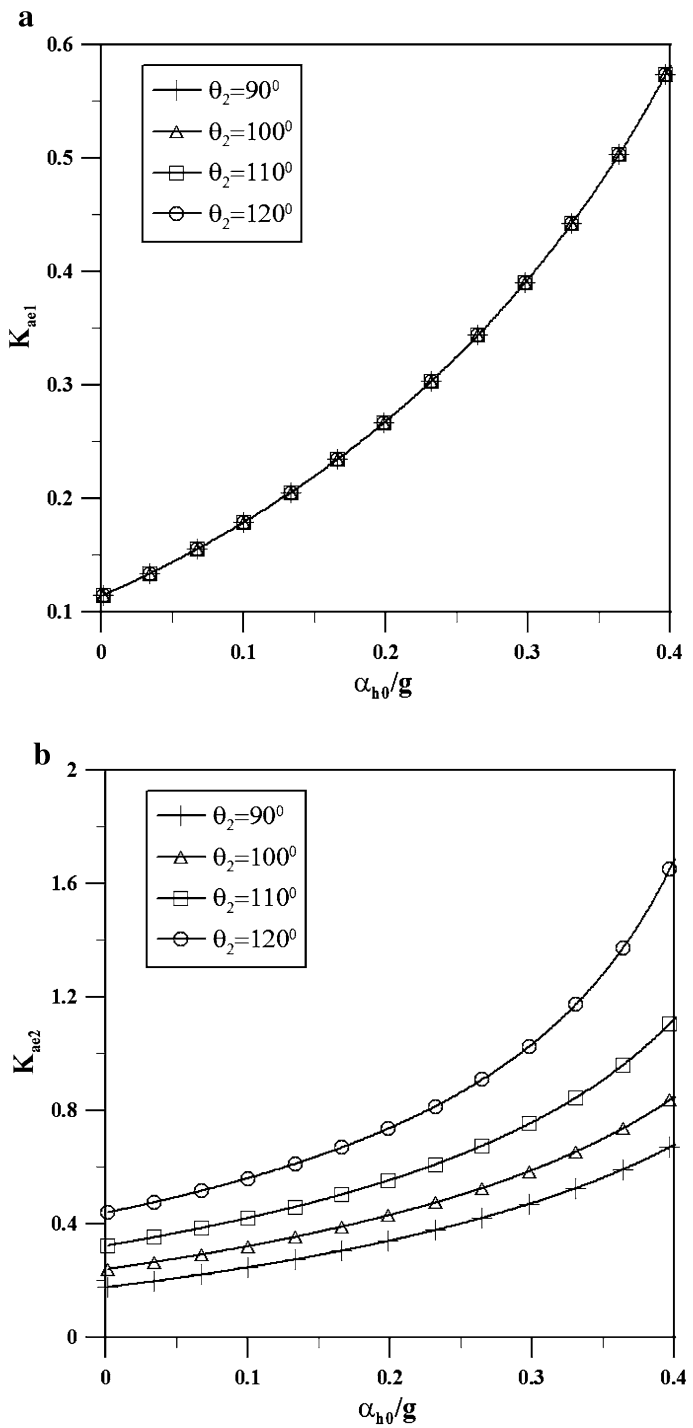

Fig. 9 Effect of inclination of bottom segment on active earth pressure coefficients [for $H_1/H = 1/3$, $\varphi = 40°$, $\delta = 0.5\,\varphi$, $\theta_2 = 100°$, $|a_{v0}| = 0.5a_{h0}$, $\omega_s H/V_s = 2$, $D = 30\%$ and $\omega_p/\omega_s = 1$]. **a** K_{ae1}, **b** K_{ae2}

Effect of P-wave and S-wave frequency ratio

The effect of ratio of angular frequencies of P-wave and S-wave is investigated in Fig. 10. It is observed that both K_{ae1} and K_{ae2} increase with increase in ω_p/ω_s. The deviations are prominent towards higher values of a_{h0}/g. It is noted that K_{ae1} and K_{ae2} increase about 16.3 and 17.15%, respectively, when ω_p/ω_s increases from 1 to 1.2 at $a_{h0}/g = 0.35$.

Seismic active earth pressure distribution

Following subsections describe the effect of various parameters on seismic active earth pressure distribution along the height of the wall for both segments.

Effect of damping ratio

With the increase in damping ratio, the normalized seismic active earth pressure decreases due to dissipation of energy in the soil media. This phenomenon has been illustrated in Fig. 11. For example, an increase in damping ratio from 10 to 30% at $z/H = 0.9$ earth pressure reduces by 7.2%.

Effect of horizontal and vertical acceleration

The effect of horizontal seismic acceleration and vertical seismic acceleration on seismic active earth pressure distribution has been illustrated in Figs. 12 and 13, respectively. It is found that the lateral earth pressure gets affected most significantly with a_{h0}/g as compared to any other parameter. For example, with an increase in a_{h0}/g from 0.2 to 0.3 (50% increase), the earth pressure increase about 82.6% at $z/H = 0.9$. On the other hand, vertical seismic force has only a marginal effect on normalized active pressure distribution as noted from Fig. 13. This is obvious that the horizontal inertia controls the lateral earth pressures largely compared to the vertical inertia.

Effect of soil friction angle

The effect of soil friction angle on seismic active earth pressure distribution has been shown in Fig. 14. It is noticed that the magnitude of active earth pressure decreases with increase in soil friction angle. As in the retaining wall with bilinear backface there is sudden change in slope of wall along depth so a discontinuity occurs in the pressure distribution at $z/H = 0.3$ which is also reported in previous study by Kolathayar and Ghosh [7].

Effect of inclination angle

Figure 15 shows the variation of normalized active earth pressure distribution for different values of θ_1 and θ_2. It can be seen that active earth pressure increase with increase in θ_1 and θ_2 due to increase in backfill weight. With same increase in θ_1 and θ_2, weight of the lower segment increases more than the upper segment so the difference in pressure in upper and lower segment at the discontinuity point increase with equal increase in θ_1 and θ_2.

Failure plane angles

As the results presented in the previous sections indicate that parameters such as horizontal seismic coefficient, friction angle, and damping of the soil have significant effect

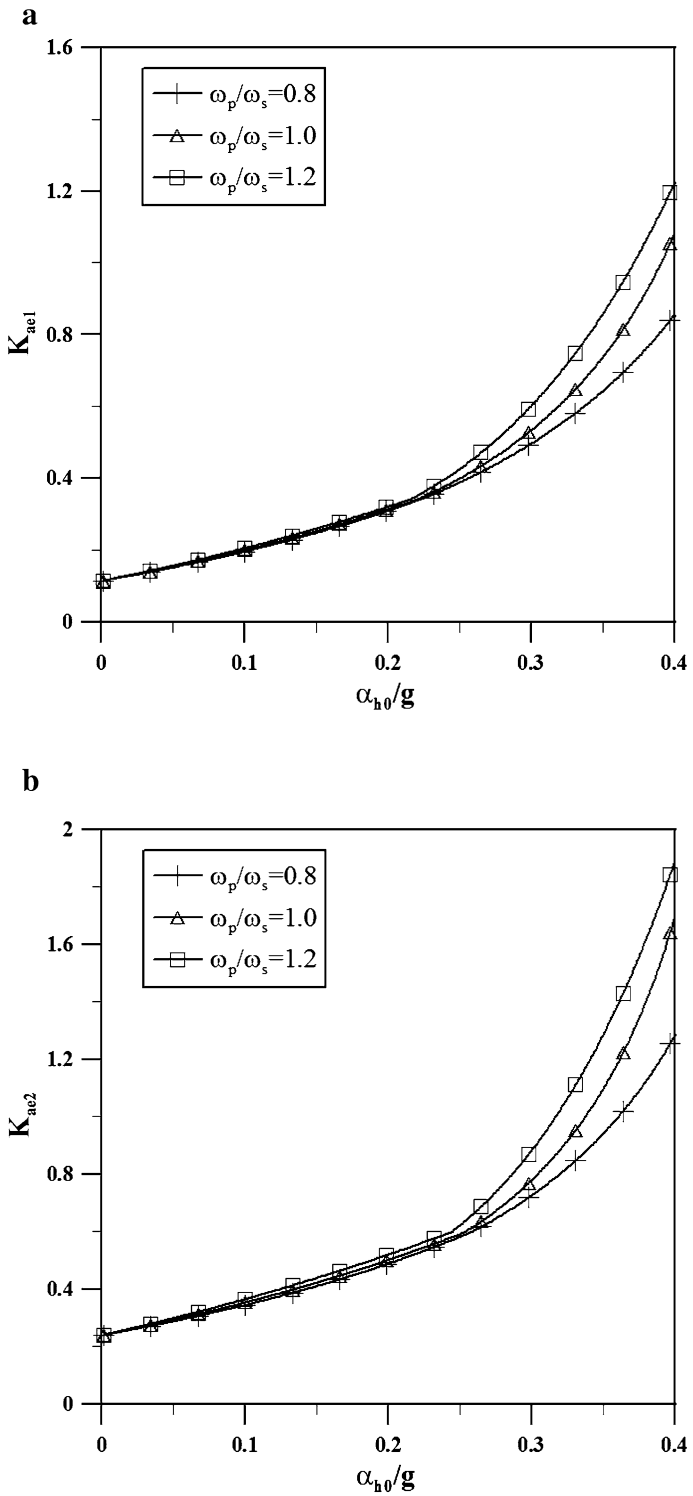

Fig. 10 Effect of ratio of angular frequencies of P-wave and S-wave on earth pressure coefficients [for $H_1/H = 1/3$, $\varphi = 40°$, $\delta = 0.5\,\varphi$, $\theta_1 = 75°$, $\theta_2 = 100°$, $|a_{v0}| = 0.5a_{h0}$, $\omega_s H/V_s = 2$ and $D = 10\%$]. **a** K_{ae1}, **b** K_{ae2}

on the active earth pressure coefficient and the lateral pressure distribution, an effort is made to examine the effect of these three parameters on the failure plane angles of both segments of the wall. Figure 16 shows the variation of failure plane angles, α_1 and α_2

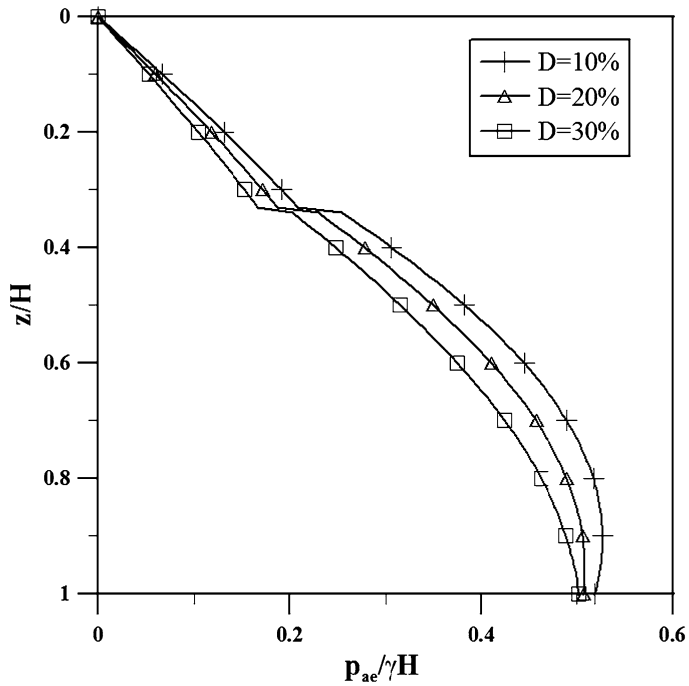

Fig. 11 Normalized active earth pressure distribution for different values of damping ratio [for $H_1/H = 1/3$, $\theta_1 = 75°$, $\theta_2 = 100°$, $\varphi = 30°$, $\delta = \varphi$, $a_{h0}/g = 0.2$, $|a_{v0}| = 0.5a_{h0}$, $\omega_s H/V_s = 2$ and $\omega_p/\omega_s = 1$]

with varying horizontal acceleration and damping ratio. It is noted that with increasing damping ratio, both angles show decreasing trend. It is very interesting to note that there is a sudden decrease in failure angle when a_{h0}/g is around 0.25 for 10 and 20% damping, whereas for 30% damping, there is no such abrupt change. The reason may that, at the point of sudden change, the direction of Q_v changes for critical active thrust. For a damping ratio of 30%, the influence of direction of Q_v becomes negligible (as also mentioned in the previous section), which leads to a smooth variation in the failure angle unlike the lower damping cases. Figure 17 shows the variation of α_1 and α_2 with φ. It is observed that both failure angles show increasing trend with increasing φ.

Comparison of results with previous studies

Table 1 presents the comparison between Greco [5], Kolathayar and Ghosh [7] and the present study for estimating K_{ae1} and K_{ae2} for a case where $H_1/\mathrm{H} = 1/2$, $\theta_1 = 75°$ $\theta_2 = 105°$, $\varphi = 36°$, $\delta = 18°$, $|a_{v0}| = 0.5a_{h0}$, $\omega_p/\omega_s = 1$. Greco [5] used a pseudo-static method, where as Kolathayar and Ghosh [7] considers a conventional pseudo-dynamic method assuming linear elastic backfill. Note that all results correspond to a normalized frequency ratio, $\omega_s H/V_s = 2$ (or in other words, $H/TV_s = 0.32$ and $H/TV_p = 0.17$, for a $V_p/V_s = 1.87$). It can be observed from Table 1 that both pseudo-static and conventional pseudo-dynamic method underestimate K_{ae1} and K_{ae2} largely. Note that this under-estimation is more prominent for higher intensity motions and low damped soil. The reason is that, for a low damped soil, frequency-dependent amplification is higher compared to a highly damped soil, which causes more deviation from the conventional methods. For example, the pseudo-static method under-estimates K_{ae1} for 17 and 46% for 0.1 and 0.3 g

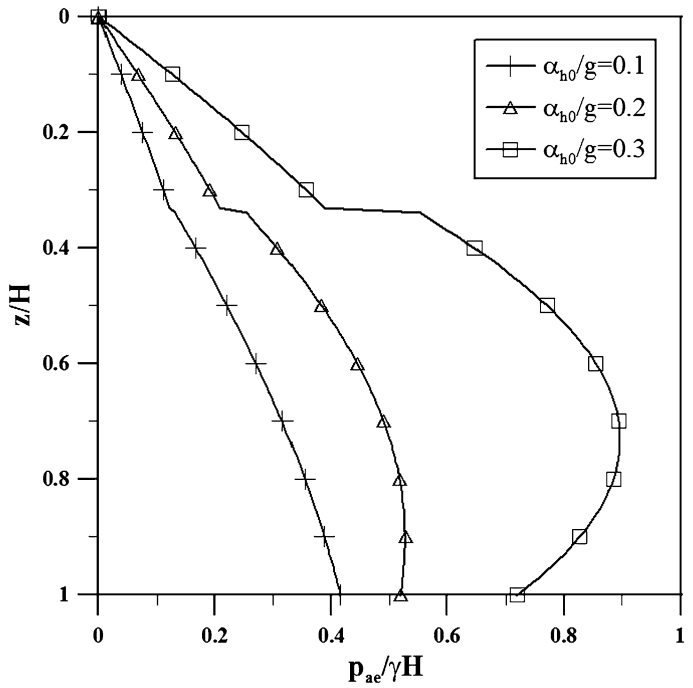

Fig. 12 Normalized active earth pressure distribution for different values of a_{h0}/g [$H_1/H = 1/3$, $\theta_1 = 75°$, $\theta_2 = 100°$, $\varphi = 30°$, $\delta = \varphi$, $|a_{v0}| = 0.5a_{h0}$, $\omega_s H/V_s = 2$, $D = 10\%$ and $\omega_p/\omega_s = 1$]

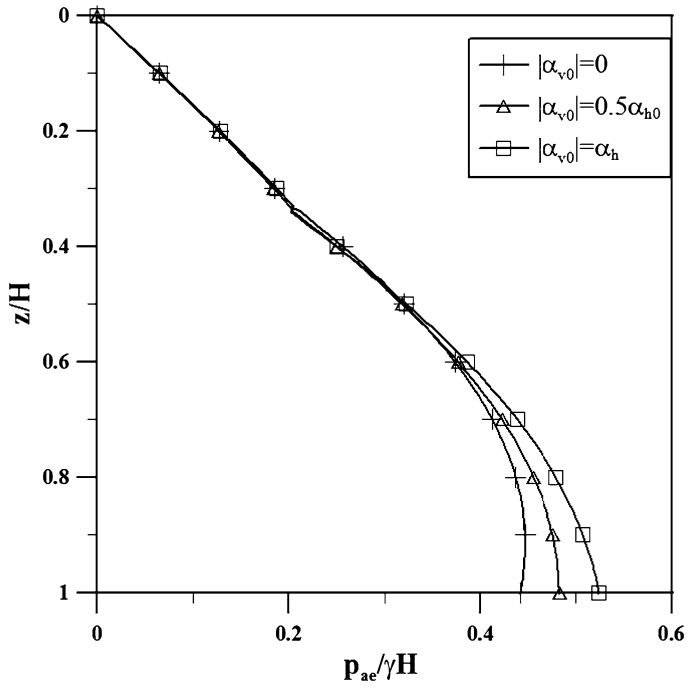

Fig. 13 Normalized active earth pressure distribution for different values of $|a_{v0}|$ [for $H_1/H = 1/3$, $\theta_1 = 75°$, $\theta_2 = 100°$, $\varphi = 30°$, $\delta = \varphi$, $a_{h0}/g = 0.2$, $\omega_s H/V_s = 2$, $D = 10\%$ and $\omega_p/\omega_s = 1$]

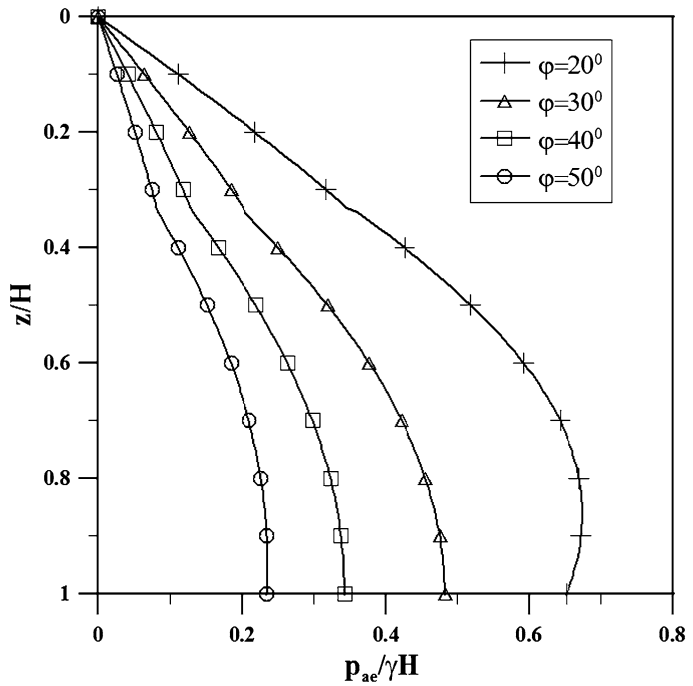

Fig. 14 Normalized active earth pressure distribution for different values of φ [for $H_1/H = 1/3$, $\delta = 0.5\varphi$, $\theta_1 = 75°$, $\theta_2 = 100°$, $a_{h0}/g = 0.2$, $|a_{v0}| = 0.5a_{h0}$, $\omega_s H/V_s = 2$, $D = 10\%$ and $\omega_p/\omega_s = 1$]

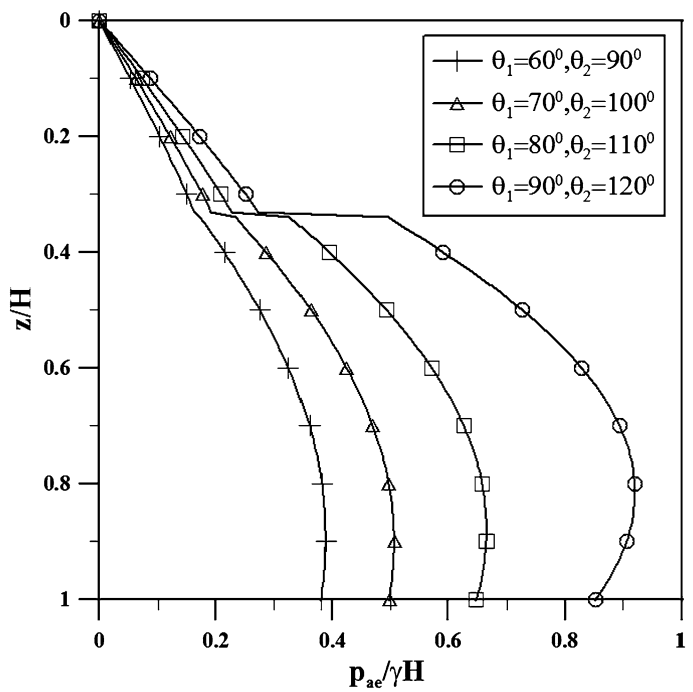

Fig. 15 Normalized active earth pressure distribution for different values of θ_1 and θ_2 [for $H_1/H = 1/3$, $\varphi = 30°$, $\delta = \varphi$, $a_{h0}/g = 0.2$, $|a_{v0}| = 0.5a_{h0}$, $\omega_s H/V_s = 2$, $D = 10\%$ and $\omega_p/\omega_s = 1$]

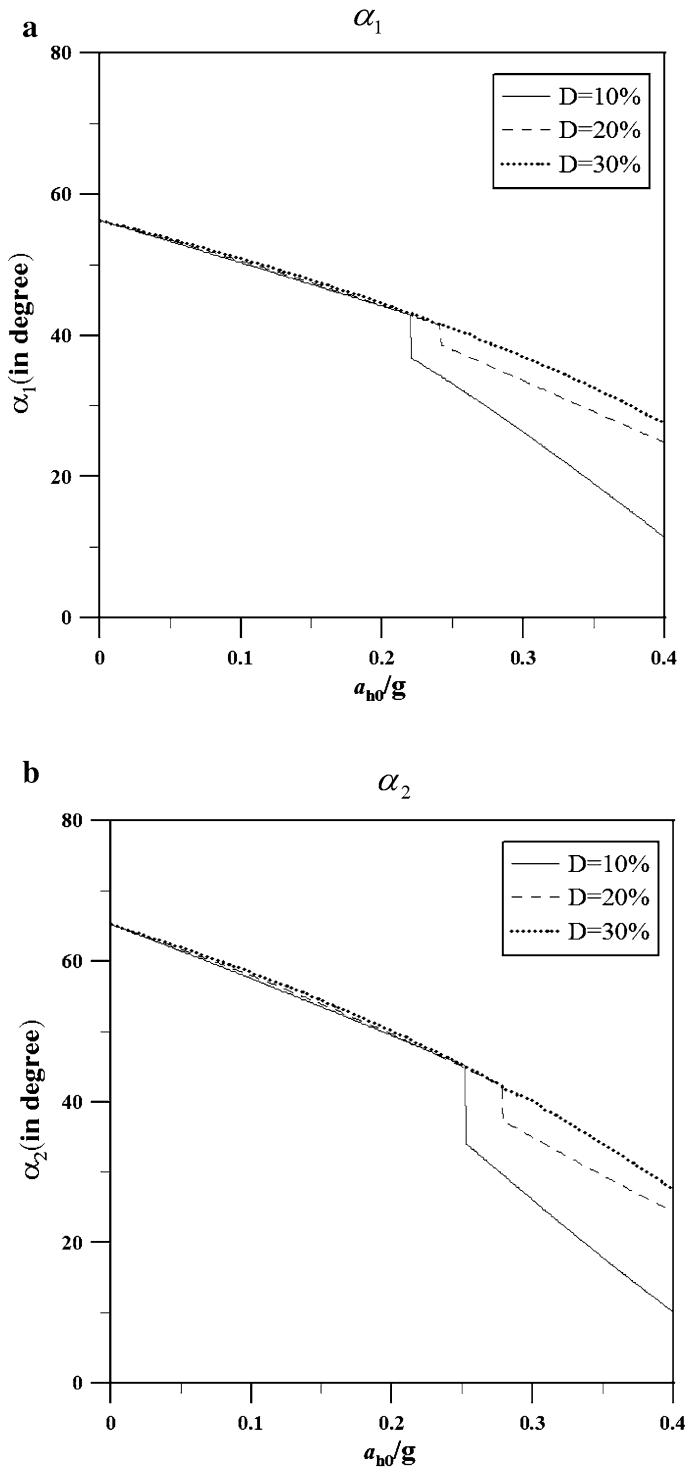

Fig. 16 Variation of **a** α_1 and **b** α_2 with a_{h0}/g [for $H_1/H = 1/3$, $\varphi = 40°$, $\delta = 0.5\,\varphi$, $\theta_1 = 75°$, $\theta_2 = 100°$, $|a_{v0}| = 0.5a_{h0}$, $\omega_s H/V_s = 2$ and $\omega_p/\omega_s = 1$]

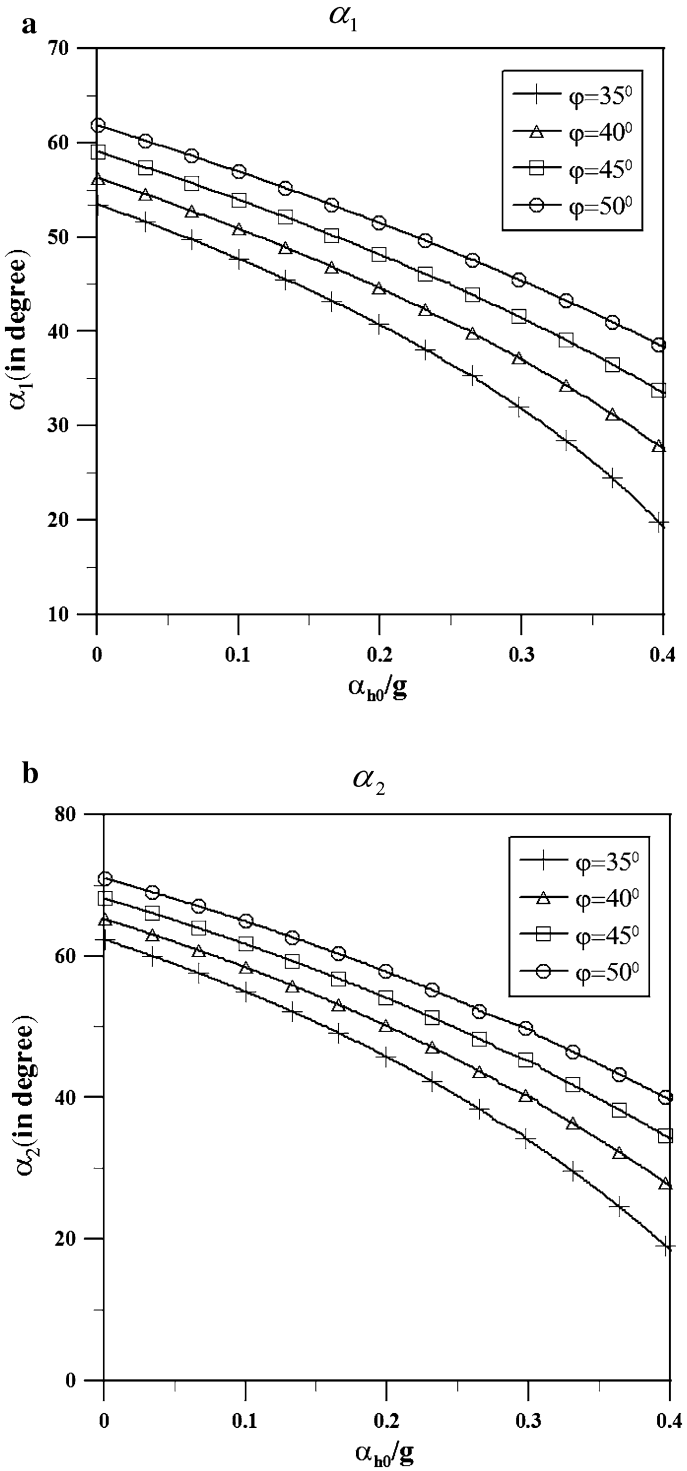

Fig. 17 Variation of **a** α_1 and **b** α_2 with a_{h0}/g [for $H_1/H = 1/3$, $\delta = 0.5\,\varphi$, $\theta_1 = 75°$, $\theta_2 = 100°$, $|a_{v0}| = 0.5a_{h0}$, $\omega_s H/V_s = 2$, $D = 30\%$ and $\omega_p/\omega_s = 1$]

Table 1 Values of active earth pressure coefficients K_{ae1} and K_{ae2} [for $H_1/H = 1/2$, $\omega_s H/V_s = 2$, $\theta_1 = 75°$, $\theta_2 = 105°$, $\varphi = 36°$, $\delta = 18°$, $|a_{v0}| = 0.5a_{h0}$ and $\omega_p/\omega_s = 1$]

a_{h0}/g	Greco [5]		Kolathayar and Ghosh [7]		Present study			
					$D = 10\%$		$D = 30\%$	
	K_{ae1}	K_{ae2}	K_{ae1}	K_{ae2}	K_{ae1}	K_{ae2}	K_{ae1}	K_{ae2}
0	0.1400	0.2600	0.1400	0.2600	0.1400	0.2600	0.1400	0.2600
0.1	0.2000	0.3000	0.1987	0.3162	0.2461	0.3737	0.2212	0.3404
0.2	0.2700	0.3500	0.2638	0.3782	0.3737	0.5234	0.3234	0.4506
0.3	0.3550	0.4030	0.3432	0.4476	0.6558	0.8629	0.4700	0.6173

motion, respectively, compared to the present study with D = 10% case. The deviations of conventional pseudo-dynamic method [7] without considering amplification in predicting this coefficient are 17 and 48% for 0.1 and 0.3 g motion, respectively.

Conclusions

This study proposes a generalized solution to estimate seismic active earth pressure on a cantilever retaining wall with bilinear backface. The proposed method is based on a modified pseudodynamic approach which overcomes the shortcomings of the existing pseudodynamic method. In order to have a more detail understanding for the application of the proposed method a parametric study has been conducted by varying the parameters such as damping ratio, frequency ratio of S-wave and P-wave, soil friction angle, wall friction angle, horizontal and vertical seismic accelera tion coefficient and wall inclination for both upper and lower portion of the wall. The results of the study shows that the natural frequency and damping of the backfill soil has significant effect on the seismic active earth pressure coefficients. Comparison with conventional pseudo-static and pseudo-dynamic methods indicate that the previous methods largely underestimate the values of K_{ae1} and K_{ae2} (as much as 48%). This under-estimation is more prominent for higher intensity motions and less-damped soil, where the soil amplification effects pose most importance. This modified pseudo-dynamic approach can further be used for design of bilinear retaining structures.

Authors' contributions
OR carried out the analysis; PRC helped in the analysis and writing of the manuscript. Both authors read and approved the final manuscript.

Author details
[1] Department of Civil Engineering, Indian Institute of Science, Bangalore, India. [2] Department of Civil Engineering, Indian Institute of Technology Kanpur, Kanpur, India.

Competing interests
The authors declare that they have no competing interests.

Received: 28 August 2015 Accepted: 4 February 2017
Published online: 07 March 2017

References

1. Bellezza I (2015) Seismic active earth pressure on walls using a new pseudo-dynamic approach. Geotech Geol Eng. doi:10.1007/s10706-015-9860-1
2. Clayton CR, Woods RI, Bond AJ, Milititsky J (2014) Earth pressure and earth-retaining structures. CRC Press, Boca Raton
3. Choudhury D, Nimbalkar SS (2006) Pseudo-dynamic approach of seismic active earth pressure behind retaining wall. Geotech Geol Eng 24(5):1103–1113

4. Das BM (1993) Principles of soil dynamics. PWS-KENT Publishing Company, Boston
5. Greco VR (2007) Analytical earth thrust on walls with bilinear backface. Proc Inst Civil Eng Geotech Eng 160(1):23–29
6. Ishibashi I, Zhang X (1993) Unified dynamic shear moduli and damping ratios of sand and clay. Soils Found 33(1):182–191
7. Kolathayar S, Ghosh P (2009) Seismic active earth pressure on walls with bilinear backface using pseudo-dynamic approach. Comput Geotech 36(7):1229–1236
8. Kramer SL (1996) Geotechnical earthquake engineering. Prentice Hall, New Jersey
9. Rahaman O (2015) Various aspects of seismic active pressure on retaining walls using pseudo-dynamic method. M-Tech thesis, Indian Institute of Technology, Kanpur
10. Sadrekarimi A, Ghalandarzadeh A, Sadrekarimi J (2008) Static and dynamic behavior of hunchbacked gravity quay walls. Soil Dyn Earthq Eng 28(2):99–117
11. Seed HB, Wong RT, Idriss IM, Tokimatsu K (1986) Moduli and damping factors for dynamic analyses of cohesionless soils. J Geotech Eng ASCE 112(11):1016–1032
12. Sokolovskii VV (1960) Statics of soil media. Butterworths Scientific Publications, London
13. Steedman RS, Zeng X (1990) The influence of phase on the calculation of pseudo-static earth pressure on a retaining wall. Geotechnique 40(1):103–112
14. Yuan C, Peng S, Zhang Z, Liu Z (2006) Seismic wavepropagation in Kelvin–Voigt homogeneous visco-elasticmedia. Sci China Ser D Earth Sci 49(2):147–153